nature communications

Article

https://doi.org/10.1038/s41467-024-51487-3

Generation of human iPSC-derived 3D bile duct within liver organoid by incorporating human iPSC-derived blood vessel

Received: 9 March 2024

Accepted: 6 August 2024

Published online: 28 August 2024

Check for updates

Erica Carolina[1,2], Yoshiki Kuse[1], Ayumu Okumura[1,2], Kenji Aoshima[1,2], Tomomi Tadokoro[3], Shinya Matsumoto[1], Eriko Kanai[1], Takashi Okumura[1], Toshiharu Kasai[1], Souichiro Yamabe[1,2], Yuji Nishikawa[4], Kiyoshi Yamaguchi[5], Yoichi Furukawa[5], Naoki Tanimizu[1] ✉ & Hideki Taniguchi[1,3] ✉

In fetal development, tissue interaction such as the interplay between blood vessel (BV) and epithelial tissue is crucial for organogenesis. Here we recapitulate the spatial arrangement between liver epithelial tissue and the portal vein to observe the formation of intrahepatic bile ducts (BDs) from human induced pluripotent stem cells (hiPSC). We co-culture hiPSC-liver progenitors on the artificial BV consisting of immature smooth muscle cells and endothelial cells, both derived from hiPSCs. After 3 weeks, liver progenitors within hiPSC-BV-incorporated liver organoids (BVLO) differentiate to cholangiocytes and acquire epithelial characteristics, including intercellular junctions, microvilli on the apical membrane, and secretory functions. Furthermore, liver surface transplanted-BVLO temporarily attenuates cholestatic injury symptoms. Single cell RNA sequence analysis suggests that BD interact with the BV in BVLO through TGFβ and Notch pathways. Knocking out JAG1 in hiPSC-BV significantly attenuates bile duct formation, highlighting BVLO potential as a model for Alagille syndrome, a congenital biliary disease. Overall, we develop a novel 3D co-culture method that successfully establishes functional human BDs by emulating liver epithelial-BV interaction.

Bile ducts (BD) specifically develop around the liver's large blood vessel (BV) called portal vein and are responsible for draining bile secreted by hepatocytes into the intestine[1]. Cholangiocytes, the epithelial component of intrahepatic BD (IHBD), are differentiated from hepatoblasts—bipotential fetal liver progenitor cells—and are specialized in secretory function. The structural dysfunction of IHBD prevents bile excretion and resulting in "cholestasis"—causing the liver accumulation of bile components such as bile acids, bilirubin, cholesterol, and phospholipids—leading to a severe liver tissue damage[2]. Our laboratory has developed a liver organoid from human induced pluripotent stem cell (hiPSC)-derived liver progenitor cells, mesenchymal cells (MCs), and endothelial cells (ECs)[3–5], though it lacked the bile drainage system. hiPSCs-organoid technology has been employed to develop IHBD-like cystic structures consisting of cholangiocytes with secretory functions[6–10]. However, considering BV-BD interaction is crucial for IHBD development[11], developing an approach to reconstruct human BDs around BV ex vivo is crucial to understand the etiology of aberrant formation of biliary structures in human newborns.

[1]Division of Regenerative Medicine, The Institute of Medical Science, The University of Tokyo, Tokyo, Japan. [2]Department of Computational Biology and Medical Sciences, Graduate School of Frontier Sciences, The University of Tokyo, Kashiwa, Chiba, Japan. [3]Department of Regenerative Medicine, Yokohama City University Graduate School of Medicine, Kanagawa, Japan. [4]Division of Tumor Pathology, Department of Pathology, Asahikawa Medical University, Asahikawa, Hokkaido, Japan. [5]Division of Clinical Genome Research, The Institute of Medical Science, The University of Tokyo, Tokyo, Japan.
✉e-mail: tanimizu@g.ecc.u-tokyo.ac.jp; rtanigu@g.ecc.u-tokyo.ac.jp

Here we analyzed the spatial relationship between the portal vein (PV) and the primitive IHBDs, discovering that SM22$^+$ immature smooth muscle cells (imSMCs) are in contact with CK19$^+$SOX9$^+$ cholangiocytes in the human fetal liver. We hypothesized that imSMCs have pivotal roles in early BD development and thus, we induced imSMCs from hiPSCs. By incorporating an artificial BV containing imSMCs and ECs, both are derived from hiPSCs, we successfully generated BD structures in hiPSC-BV incorporated liver organoid (BVLO). Given that the molecular pathways regulating BV-BD interaction are emulated in BVLO, this culture system offers a viable ex vivo model for human congenital biliary diseases.

Results

The correlation between the portal vein vascular smooth muscle cells and the early stage of cholangiocyte differentiation

Differentiation of cholangiocytes from bipotential liver progenitors highly depends on a specific BV called PV[12,13]. Vascular SMCs of PV (PV-SMCs) have crucial roles in BD development as evidenced by the observation that knockout of Jagged1 (JAG1), a Notch ligand, in PV-SMCs leads to abnormal BD development[11]. According to the previous findings[14] that smooth muscle protein 22 (SM22) and α-smooth muscle actin (αSMA) serve as early and late markers for vascular SMCs respectively, we performed immunostaining of embryonic day 15.5 (E15.5) mouse liver to investigate possible correlation between the differentiation status of PV-SMCs and BD development. Our result demonstrated that PV-SMCs thoroughly express SM22 (Supplementary Fig. 1A), whereas strong αSMA expression is mainly observed in the hilum area but notably faint in the peripheral area (Fig. 1A and Supplementary Fig. 1B). As BD morphogenesis proceeds from the hilum outward to the periphery[15,16] where PV-SMCs characterized by SM22$^+$αSMA^{low}, it is noteworthy that cholangiocytes in the peripheral tissue may be potentially derived from hepatoblasts undergone recent differentiation. In addition, our immunostaining of human fetal liver section at gestation week 15 (GW15) demonstrated that SOX9$^+$ and CK19$^+$ ductal plates without clear lumen emerge next to SM22$^+$SMA^{low} SMCs, whereas those adjacent to SM22$^+$αSMA^{high} SMCs are associated with the luminal formation (Fig. 1B). Based on these results, we hypothesized that PVs undergo maturation from αSMA^{low} to αSMA^{high} status as they extend from the hilum towards the periphery. Importantly, immature SMCs (imSMCs) in the periphery area are correlated with the induction of cholangiocyte from bipotential progenitors. To further support our developmental observation, we extracted the mesenchymal cell cluster characterized by the expression of Pdgf receptor β, Vimentin, Desmin, and Collagen 1a1, from human GW9-12 fetal liver single cell transcriptome data[17] (Supplementary Dataset 1) and further identified vascular SMC-related genes expressing cluster (cluster 1 in Fig. 1C), which is characterized by the expression of *Transgelin* (*TAGLN*) (gene coding SM22), *Actin alpha 2* (*ACTA2*) (gene coding αSMA), and *JAG1*. In consistent with the dot plot (Middle panel of Fig. 1C), αSMA$^+$ cells exist in all clusters on the feature plot, whereas most of SM22$^+$ and JAG1$^+$ cells are in cluster 1. To assess the co-expression of those genes, we highlighted cells in the feature plot that express *TAGLN*, and *JAG1* alongside *αSMA* at relatively low level (<4), indicating that JAG1 is expressed more in SM22$^+$αSMA^{low} cells than in SM22$^+$αSMA^{high} cells.

Taken together, these data suggest that the immature status of PV-SMCs is correlated with the early stage of BD development.

Generation of immature SMC containing hiPSC-blood vessels (hiPSC-BV)

Next, we adapted the previously reported differentiation protocol for inducing vascular SMC from hiPSC[18] (Fig. 1D) to investigate whether varying maturation stages of hiPSC-SMC affect its capability in triggering cell fate decision of bipotential liver progenitors towards cholangiocytes, when incorporated as the component of hiPSC-BV.

During hiPSC-SMC differentiation, our immunofluorescence and quantitative PCR (qPCR) data showed that SM22$^+$αSMA^{low} cells emerge on day 6 whereas SM22$^+$αSMA^{high} cells emerge on day 10 after differentiation (Fig. 1E). Accordingly, we utilized these two types of mesenchymal cells that emerged on day 6 and 10 of culture as hiPSC-imSMCs and hiPSC-SMCs, respectively. qPCR analysis showed that *JAG1* are highly expressed in hiPSC-imSMCs (Fig. 1F), suggesting that imSMCs may have higher potential to induce cholangiocyte differentiation.

3D co-culture system combining hiPSC-BV with hiPSC-liver organoid induces the generation of hiPSC-BD

Building on insights from previous studies[15,16] and data presented in Fig. 1, which highlight the critical role of BV and liver progenitor cell interactions in BD development, we establish a culture system using the artificial BV. In line with the prevalent use of biomaterial scaffold like collagen-1 gel for creating artificial BV in tissue-engineering[19], this study utilized collagen-1 scaffold to generate hiPSC-BV. The hiPSC BV structure consists of hiPSC-imSMCs as the outer layer and hiPSC-ECs as the delineating inner layer (Fig. 2A).

As a source of bipotential liver progenitor cells, we used hiPSC-hepatic endoderm cells (HEs) co-cultured with hiPSC-MCs and ECs, which possess bipotential capabilities, as evident by their ability to differentiate into either hepatocyte or cholangiocyte depending on its culture condition[20]. To establish the 3D culture system, we further utilized a sheet-shaped aggregated liver organoid. This sheet-shaped liver organoid was designated to be overlaid around the hiPSC-BV tube, after which the extracellular matrix (ECM) was applied to coat the outer layer. In this study, the sheet-shaped liver organoid, which overlaid around the collagen matrix tube, was used as the control group. The 3D co-culture was performed for 3 weeks. However, our macroscopic imaging and immunostaining observations suggest that hiPSC-BV containing only cells was inadequate for inducing cholangiocyte differentiation (Fig. 2B, C).

Previous studies show that the activation of TGFβ and Notch signal in liver progenitors is important for cholangiocyte differentiation[21,22]. In addition, not only that laminin 511 is necessary to form mouse mature BD[23], it is also considered as the most suitable ECM component to induce cholangiocyte differentiation from hiPSC-hepatoblast[24]. Therefore, we optimized hiPSC-BV composition by adding JAG1, TGFβ1, and laminin 511 recombinants. Following co-culture of sheet-shaped liver organoid with hiPSC-BV that contains JAG1/TGFβ1/Laminin 511 recombinant proteins, kusabira orange-labeled HE (KO-HE)-derived cells were macroscopically localized into a mesh-like structure (Fig. 2B). Immunostaining analysis demonstrated that HE-derived cells form CK19$^+$ BD-like luminal structure (Fig. 2C). We named this optimized condition as blood vessel incorporated liver organoid (BVLO). Of note, when SMCs instead of imSMCs were used to generate the hiPSC-BV, KO-HE did not form BD structures.

Hematoxylin & Eosin (H&E) staining and quantification suggested significant BD lumen formation within BVLO (Fig. 2D, E). Time course analysis revealed that, at early stage, duct structures are double positive for CK19 and HNF4α, whereas those at day 21 are CK19$^+$HNF4α$^-$ (Supplementary Fig. 2) showing overtime maturation of BD.

To investigate how BVLO's cell component changes gene expression over time, we performed qPCR analysis on each cell type after sorting by flow cytometry (Fig. 2F). First, GFP-tagged ECs and GFP-tagged SMCs were used to distinguish hiPSC-BV cells from liver-organoid cells. Next, APC-CD31 staining was performed to segregate between these two cell types. qPCR analysis of SMC-related gene expression (αSMA, SM22, JAG1) and EC-related gene expression (TGFβ1, TGFβ2, TGFβ3, VE-CAD) suggested no significant change in both BV-cell population characters at different time points throughout the co-culture (Fig. 2F).

https://doi.org/10.1038/s41467-024-51487-3

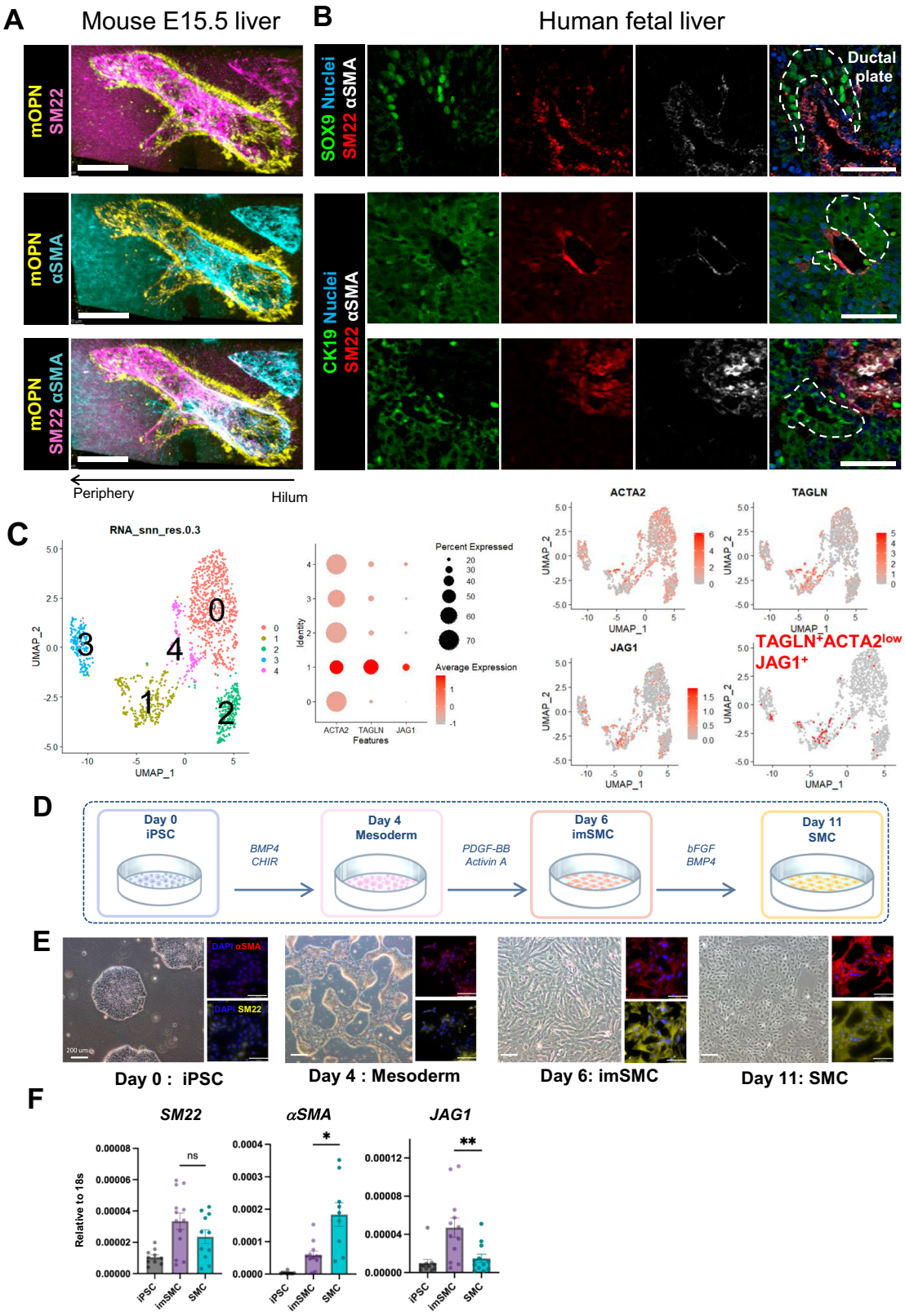

Next, to better understand the gene expression changes during the cholangiocyte differentiation from HE cells, the KO$^+$ cells in BVLO were sorted by flow cytometry, and expression of cholangiocyte lineage marker genes was analyzed by qPCR. The gene expressions related to the epithelial cytoskeleton (*KRT7*) and BD transporter (*GPBAR1*) were significantly upregulated (Fig. 2F), which supports our argument that fraction of HE cells differentiate into cholangiocytes in BVLO. In addition to that, other BD transporters (*AQP1* and *CFTR*) gene expression increase trend could also be observed.

We further examined duct structures in BVLO by immunofluorescence analysis (Fig. 2G). The data indicated BD-like structure in BVLO exhibits positive expression of BD markers (CK19, CK7, GRHL2), tight junction (ZO-1, CLDN4), epithelial marker (E-cad), and apico-basal polarization markers (F-actin, βCAT, RDX) (Fig. 2G and Supplementary

Fig. 1 | The developmental gradient of PV-SMC along the hilum-periphery axis suggests a potential correlation with the earliest differentiation of cholangiocyte progenitor cells. A Wholemount immunofluorescence analysis of OPN$^+$ cholangiocytes and PV-SMC at E15.5. SM22$^+$ vascular SMCs delineates the PV thoroughly, with a gradient of αSMA expression from high to low at the periphery, suggesting variable SMC maturation stages in BD development. Scale bars: 200 μm. Two-photon imaging was performed independently on biological replicates ($n = 2$) and the representative image is shown in this panel. Confocal microscope imaging also performed ($n = 3$). **B** Immunotaining of PV-SMC and ductal plates in human fetal liver slice at GW15, based on the placental villi morphology. Ductal plates highlighted with dotted lines. Three to four PV areas per section ($n = 2$) were examined. Scale bar: 50 μm. **C** scRNA-seq analysis of mesenchymal cell populations in human fetal liver at GW9 ~ 12, identifying five distinct clusters. Dot plot shows cluster 1 contains *ACTA2*(gene coding αSMA)$^+$*TAGLN* (gene coding SM22)$^+$*JAG1*$^+$ cells. *ACTA2*$^+$, *TAGLN*$^+$, and *JAG1*$^+$ cells are highlighted on each feature plot, whereas *TAGLN*$^+$*JAG1*$^+$ and *ACTA2*^{low} (expression level < 4) cells are highlighted in the lower right feature plot indicating *TAGLN*$^+$ *ACTA2*^{low} *JAG1*$^+$ are enriched in cluster 1. **D** Schematic illustration of stepwise induction process of SMCs from hiPSCs. **E** Differentiation of human iPSC-derived smooth muscle cells in-vitro visualized through bright field imaging and immunostaining for αSMA and SM22. Scale bars: 200 μm (phase contrast) and 100 μm (fluorescence). Experiments were repeated independently more than three times with similar result. **F** qPCR analysis of the expression level of *SM22*, *αSMA*, *JAG1* of hiPSC-derived cells throughout different stages of SMCs in-vitro differentiation process. hiPSC ($n = 10$), imSMC ($n = 13$), and SMCs ($n = 11$) were cultured, independently. The boxes indicate mean expression levels while error bars represent standard deviations (SD). (SM22 expression of imSMC vs SMC, Mann-Whitney test, Statistical significance: ns, *P*-value of 0.2066; αSMA expression of imSMC vs SMC, Mann-Whitney test, Statistical significance: *P-value of 0.0148; JAG1 expression of imSMC vs SMC, Mann-Whitney test, Statistical significance: **P-value of 0.0070).

Fig. 3A). We also generated BVLOs from different hiPSC lines to show the robustness of this coculture system (Supplementary Fig. 3B).

Together, these findings show that when co-cultured with hiPSC-BV containing JAG1, TGFβ1, and Laminin 511, hiPSC-liver progenitors derived from HE differentiate into cholangiocytes forming BD-like structures.

hiPSC–bile ducts establish epithelial structures and possess secretory functions

We further evaluated the structural and functional features of BVLO-BD to determine their functionality. Immunofluorescence analysis demonstrated that within BVLO, CK19$^+$CK7$^+$ cholangiocytes surrounded an elongated lumen (Fig. 3A), indicating the formation of BD tubules from hiPSC-cholangiocytes in BVLO. We also performed 3D imaging, demonstrating that CK19$^+$ hiPSC-cholangiocytes are organized into the tubular structure (Supplementary Video 1) and that the luminal structure is sealed with tight junctions (Supplementary Video 2). Transmission electron microscopy (TEM) imaging revealed the presence of microvilli extending from the BD apical membrane into the lumen (Fig. 3B), which are not observed in LOs (Supplementary Fig. 4). TEM also identified tight-junction structures at intercellular spaces. These results indicate that hiPSC-liver progenitors establish cholangiocytes' epithelial characteristics in BVLO.

Cholangiocyte secretory functions depend on specific transporters on the apical side of the BD lumen[25]. To assess the function of BVLO-BD that localizes multi drug resistance protein 1 (MDR1) on the apical membrane (Fig. 3C), we evaluated its ability to efflux MDR1 substance rhodamine 123 (Rho123) to the lumen. Through live imaging and immunofluorescence analysis, we observed the accumulation of Rho123 in the BD lumen (Fig. 3D, E and Supplementary video 3). With verapamil (MDR1 inhibitor), we observed Rho123 is not accumulated into the BD lumen but rather localized within the BD cell (arrowheads in Fig. 3E and Supplementary video 4). This responsiveness implies that tubular BVLO-BD possesses MDR1 dependent efflux function.

In addition to the Rho123 assay, we performed the forskolin-induced swelling assay to evaluate cholangiocytes' secretory function. Previous studies have shown that the activation of cAMP synthetase by forskolin leads to the relocation of cystic fibrosis transmembrane conductance regulator (CFTR) transporter to the apical membrane, resulting in fluid accumulation within the apical lumen[26,27]. We first confirmed that CFTR is expressed on the apical membrane of BVLO-BD (Fig. 3F). Next, we divided BVLO into two parts: the first part was immediately fixed for analysis, whereas the other part was treated with forskolin. After forskolin treatment, the lumen diameter was significantly increased (Fig. 3G) and the cross-sectional area of BDs in BVLO increased by 2.5-fold on average (Fig. 3H). Collectively, hiPSC-cholangiocytes within BVLO exhibit functional epithelial intercellular junctions and secretory functions in BVLO.

Furthermore, we examined the enzymatic activities of γ-glutamyltransferase (GGT) and alkaline phosphatase (ALP), which are localized in the biliary pole of hepatocytes and in cholangiocyte and secreted into bile in the adult liver[28]. A previous study also demonstrated that their activities are maintained in cholangiocytes in vitro[29]. We observed that BVLO exhibits GGT enzymatic activity after co-culture (Fig. 3I), and BCIP/NBT staining detects the ALP activity in hiPSC-cholangiocytes that forms BD lumen within BVLO (Fig. 3J and Supplementary Fig. 5).

Together, these results indicate that spatially organized hiPSC-BDs within BVLO establish BD-specific structural and functional features.

Liver surface transplantation promotes maturation of cholangiocytes in BVLO

hiPSC-liver progenitors acquired cholangiocyte characteristics including secretory function within BVLO so far. To investigate whether cholangiocytes will further differentiate in vivo, we introduced BVLO on the liver surface of immunodeficient mice (Fig. 3K). Post-transplantation, we observed positive expression of OPN and acetylated tubulin on the apical surface, which were not detected after in vitro co-culture, suggesting advanced maturation following in vivo incubation (Fig. 3L, M). To examine possible host-graft BD connection, we utilized a common method to visualize the continuous luminal network of BD by injecting carbon ink from the extrahepatic BD (EHBD)[30] of BVLO-transplanted mice (Fig. 3N). The liver tissue injected with carbon ink was analyzed with immunofluorescence staining, and we confirmed carbon ink accumulation within the Ku80$^+$ graft area, inside the hCK7$^+$ BD lumen that is adjacent to host mOPN$^+$ IHBDs (Fig. 3O, Supplementary Fig. 6A, B). These results indicate that hiPSC-cholangiocytes in BVLO further maturated following in vivo incubation and that the transplanted BD is connected to the host IHBD.

BVLO transplantation temporarily ameliorates symptoms of cholestatic disease

Our data demonstrate that the host-graft BD connection was established post-transplantation, leading us to hypothesize a possibility that BVLO transplantation could ameliorate symptoms of cholestatic disease. We performed bile duct ligation (BDL) on immunodeficient mice to induce cholestatic liver injury through the bile accumulation within the liver tissue. Then, BVLO was transplanted onto the liver surface right after BDL (Fig. 4A). Jaundice was clearly induced following BDL (Fig. 4B and Supplementary Fig. 6C). The sham-operated mice exhibited a mean survival of merely 4 days, whereas mice receiving BVLO-transplantation demonstrated a significant improvement of the average survival to 7 days (Fig. 4C). Since most of the sham-operated mice could not survive after 1 week, the liver injury serum marker was examined on day three after transplantation. In comparison with the sham-operated mice, BVLO-transplanted mice showed lesser elevation in direct and total

https://doi.org/10.1038/s41467-024-51487-3

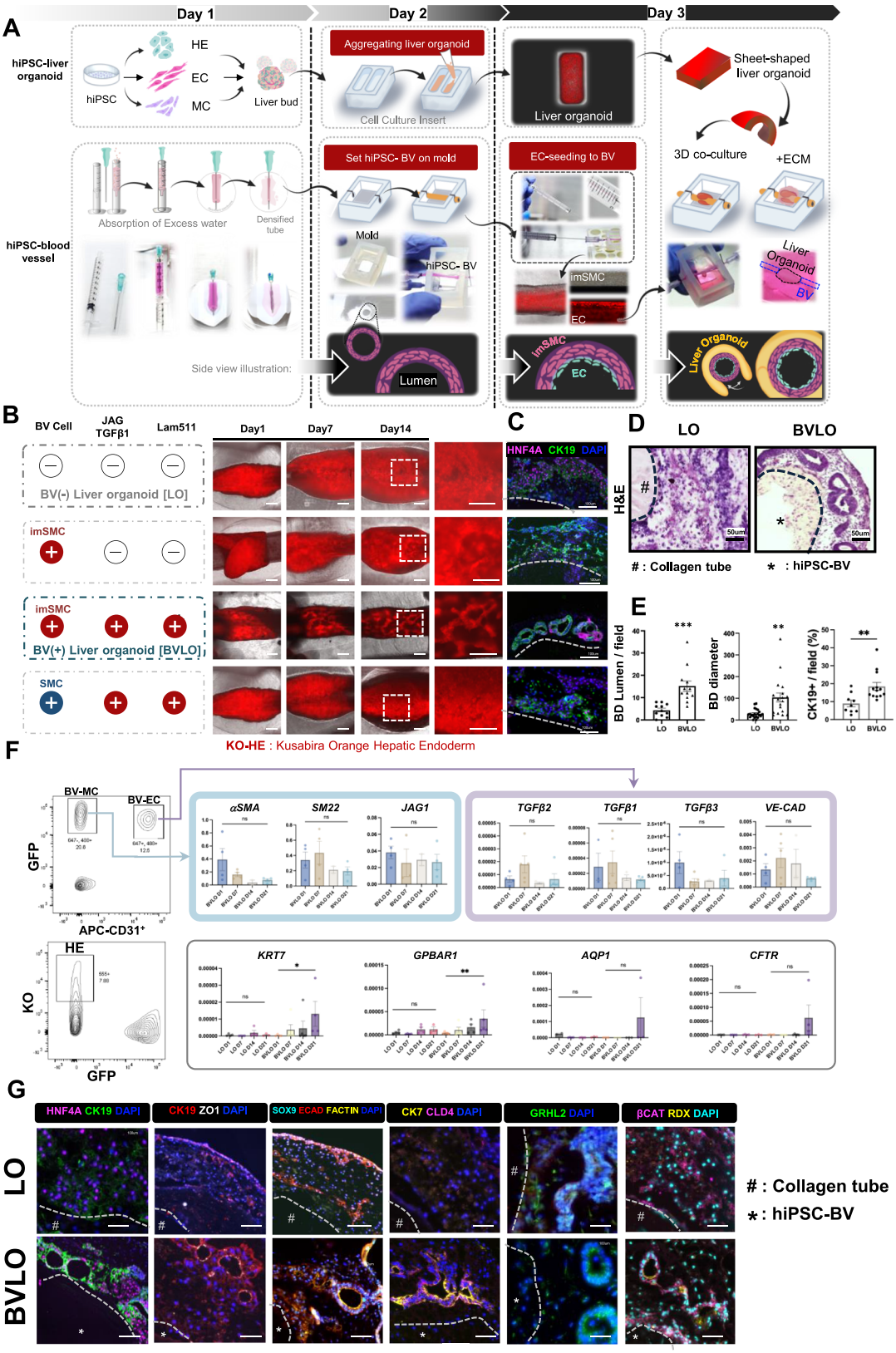

bilirubin (D-Bil and T-Bil) (Fig. 4D) with fewer mice body weight reduction (Fig. 4E). Finally, our thick-sliced transplanted liver revealed that the luminal space of graft-BDs become larger (Fig. 4F, G). We assumed that the external biliary structure in BVLO upon host-graft connection, may serve as an auxiliary bile reservoir for the recipient liver, thereby facilitating a temporary alleviation of cholestasis symptoms.

scRNAseq analysis suggests BV-BD interaction through TGFβ and Notch pathways in BVLO

BVLO culture protocol was designed to emulate PV-BD interaction in developing liver by culturing the sheet-shaped hiPSC-liver organoid around hiPSC-BV. Previous mouse studies demonstrated that TGFβ and Notch signals mediate the PV-BD interaction. The latter signal is

Fig. 2 | Optimized human iPSC-derived blood vessel induces tubular-like bile duct structure within hiPSC-blood vessel incorporated liver organoid (BVLO). **A** Experimental workflow for generating iPSC-derived blood vessel on collagen-1 scaffold. **B** Localization of Kusabira Orange (KO)-HE cells in optimized co-culture shown in merged phase-contrast (grayscale), and KO fluorescence (red) images. Scale bar, 500 μm. Culture in each condition was repeated independently more than three times with similar results. **C** Immunofluorescence of CK19 (cholangiocyte) and HNF4α (hepatoblast) at day 14 under different conditions. Scale bar, 100 μm. Three to four fields of view from over five independent organoid samples were analyzed. **D** H&E staining of co-cultured liver organoid with BV (BVLO) or without hiPSC-BV (LO). **E** Quantification of BD lumen number, diameter, and $CK19^+$ ratio per field for BVLO and LO. Three to four fields of view from over five independent organoids were analyzed (Error bars: SEM, Two-tailed unpaired T-test, Statistical significance: ***, **, **P-value of 0.0004, 0.0006, 0.0058). **F** FACS sorting of GFP-hiPSC-MC (GFP^+CD31^-) or GFP-hiPSC-EC (GFP^+CD31^+) populations post-dissociation, followed by qPCR analysis of SMC markers (*αSMA*, *SM22*, *JAG1*). Living cells were identified by propidium iodide negativity and categorized by GFP and CD31 expression level (Statistical analysis using Two-tailed Mann-Whitney; n.s, n.s, n.s; *P*-value of 0.1143; 0.4329; 0.3429); Endothelial markers (*TGFB1, TGFB2, TGFB3, CDH5*) (Internal control 18S rRNA, n.s, n.s, n.s, n.s; *P*-value of 0.7302; 0.7857; 0.3429; 0,3429). KO-HE sorted from BVLO post-dissociation. Cell isolation for LO and BVLO was performed at various days (LO day 1 ($n = 4$), day 7 ($n = 4$), day 14 ($n = 4$), day 21 ($n = 3$); BVLO day 1 ($n = 4$), day 7 ($n = 5$), day 14 ($n = 5$), day 21 ($n = 4$)). Cholangiocyte markers (*KRT7*, *GPBAR1*, *AQP1*, *CFTR);* (Statistical significance for *KRT7*, ns, *P-value of 0.8571, 0.0286; *GPBAR* n.s, **P-value of 0.4000, 0.0079; *AQP1* n.s, n.s, *P*-value of 0.2000, 0.0571; *CFTR* n.s, n.s, *P*-value of 0.6286, 0.1143). Error bars: SEM. **G** Immunostaining of cholangiocyte (CK19, SOX9, CK7, GRHL2), epithelial junction (ZO1, ECAD, FACTIN, CLDN4, βCAT, RDX) and hepatocyte (HNF4A). Over three fields of view from over five independent organoid samples were analyzed. Scale bar: 50 μm.

especially crucial for human BD development, as evident by the BD paucity in Alagille syndrome attributed to JAG1 or NOTCH2 mutations. However, the mechanism by which these signals are activated in human liver progenitor cells through PV-BD interaction during BD development is yet to be elucidated. To this end, we analyzed gene expression profile of organoid component cells at single cell level to reveal signals transmitting BV-BD interaction in BVLO.

scRNA-seq analysis identified hepatocytes, endothelial cells, and mesenchymal cells as well as cholangiocytes within BVLO (Fig. 5A and Supplementary Fig. 7). Next, we combined BVLO data with a publicly available scRNA-seq data of human adult liver cells (GSE192742) to demonstrate the resemblance between BVLO component cells to those of primary human liver cells. Our analysis revealed that human hepatocytes are subclustered to five subpopulations, with BVLO hepatocytes being subclustered to four of those populations. Furthermore, three distinct populations of cholangiocytes are identified, and BVLO cholangiocytes are subclustered to one of them (Fig. 5B, Supplementary Data 2 and Supplementary Fig. 8). The similarity of hepatocytes and cholangiocytes are further illustrated through a heatmap showing expression profile of hepatobiliary marker genes, highlighting the shared characteristic between corresponding cell types (Fig. 5C). Leveraging scRNA-seq data, we analyzed possible intercellular interaction by employing NicheNet[31] to extract molecular information of BV-BD interaction by designating MC or EC as "sender" cells (those providing ligands), along with cholangiocytes as "receiver" (those receiving ligands), respectively (Fig. 5D). The analysis identified the TGFβ signaling pathway as the most prominent interaction in both EC-cholangiocyte and in MC-cholangiocyte interaction, whereas JAG1-NOTCH signaling pathway appears to be predominantly activated in MC-cholangiocyte interaction. In summary, transcriptome analyses of BVLO component cells suggest that TGFβ and Notch signaling pathways are activated in BD, potentially induced by BV component cells (Fig. 5E).

TGFß and Notch signaling are involved in the development of hiPSC-BD

To investigate the role of identified signaling pathways in BD formation, we introduced ALK4/5/7 inhibitor (A8301) to obstruct TGFβ signaling pathway, or a γ-secretase inhibitor (DAPT, L685458) to block the NOTCH signaling in our co-culture system. The treatment of respective inhibitors resulted in complete abrogation of the BD structure formation, while the cholangiocyte differentiation was inhibited but was not entirely blocked (Fig. 6A-C). Although the NicheNet analysis of scRNA-seq data suggested that both ECs and imSMCs provide TGFβ1 (Fig. 5D), our qPCR data demonstrated that TGFβ is dominantly supplied from ECs and JAG1 from imSMCs, respectively (Fig. 1F and Supplementary Fig. 9). To examine cell-cell communication through the TGFß1 and JAG1/Notch pathway, TGFß1 was added to the hiPSC-imSMC culture and the JAG1 expression was examined. The TGFß1 recombinant addition increased the JAG1 expression of imSMC, while the A8301 treatment canceled this phenotype (Fig. 6D, E), which suggests that TGFß1 acts as an upstream of the Notch pathway by upregulating JAG1. To elucidate the role of JAG1 expression from hiPSC-BV cellular component for BD lumen formation in BVLO, we constructed hiPSC-BVs by using imSMCs derived from two clones of JAG1-knockout ($JAG1^{-/-}$) hiPSCs, alongside a JAG1 wildtype ($JAG1^{+/+}$) clone (Fig. 6F, G, Supplementary Fig. 10A, B) and then co-cultured them with liver organoid. While $JAG1^{+/+}$ hiPSC-imSMC BV account as positive control for BD formation within BVLO, our immunofluorescence analysis and $CK7^+$ lumen quantification data indicated that BVLO co-cultured with BV containing either of the two $JAG1^{-/-}$ hiPSC-derived imSMCs fail to develop BD lumen (Fig. 6H, I). Interestingly, despite the indispensable role of JAG1 in imSMCs for BD lumen formation, $JAG1^{-/-}$ hiPSC-liver progenitors were still capable of forming BD lumen in BVLO (Fig. 6J, K). This distinction underscores a differential requirement for JAG1 in the developmental processes of BD formation, highlighting the unique role of JAG1 in imSMC compared to its role in hiPSC-liver progenitors.

All in all, the signaling pathways vital for mouse BD development are also instrumental in regulating human BD development, and BVLO models that lacking JAG1 in BV-SMCs can specifically recapitulate the abnormal BD formation observed in human Alagille syndrome.

Discussion

In the present study, we generated BD structures within a hiPSC liver organoid by emulating inter-tissue interaction between PV and BD that occurs during fetal liver development. To our knowledge, this study is the first to establish a culture protocol to generate hiPSC-BD structures in the liver organoid by incorporating a large artificial BV.

Our mouse developmental observation suggests that immature SMCs play a crucial role at the initial stage of BD development. Consistently, governing the maturity of artificial BV cellular components is essential for efficient induction of 3D hiPSC-derived BD lumen structure. It is immature hiPSC-SMCs, rather than the mature SMCs, that more effectively promote cholangiocyte differentiation and facilitate hiPSC-BD lumen generation.

The hiPSC-BD in BVLO meets the phenotypic criteria of IHBD signature. Generated hiPSC-BDs demonstrate proper localization of cholangiocyte lineage-markers such as tight junction, transporters, and transcription factors, as well as MDR1-dependent directional transport of Rho123 and lumen expansion as a response against forskolin. In the current work, OPN expression was detected only after liver surface transplantation. This finding aligns with previous reports indicating that human OPN expression is pronounced in adult IHBDs but absent in fetal ones[32,33], suggesting that observed OPN expression marks a maturation process that happened after in vivo incubation. In addition to OPN, acetylated tubulin was also only detected on the apical surface of BVLO-BD exclusively after transplantation. However, the absence of primary cilia as indicated by the apical membrane localization of acetylated tubulin suggests incomplete maturation of

https://doi.org/10.1038/s41467-024-51487-3

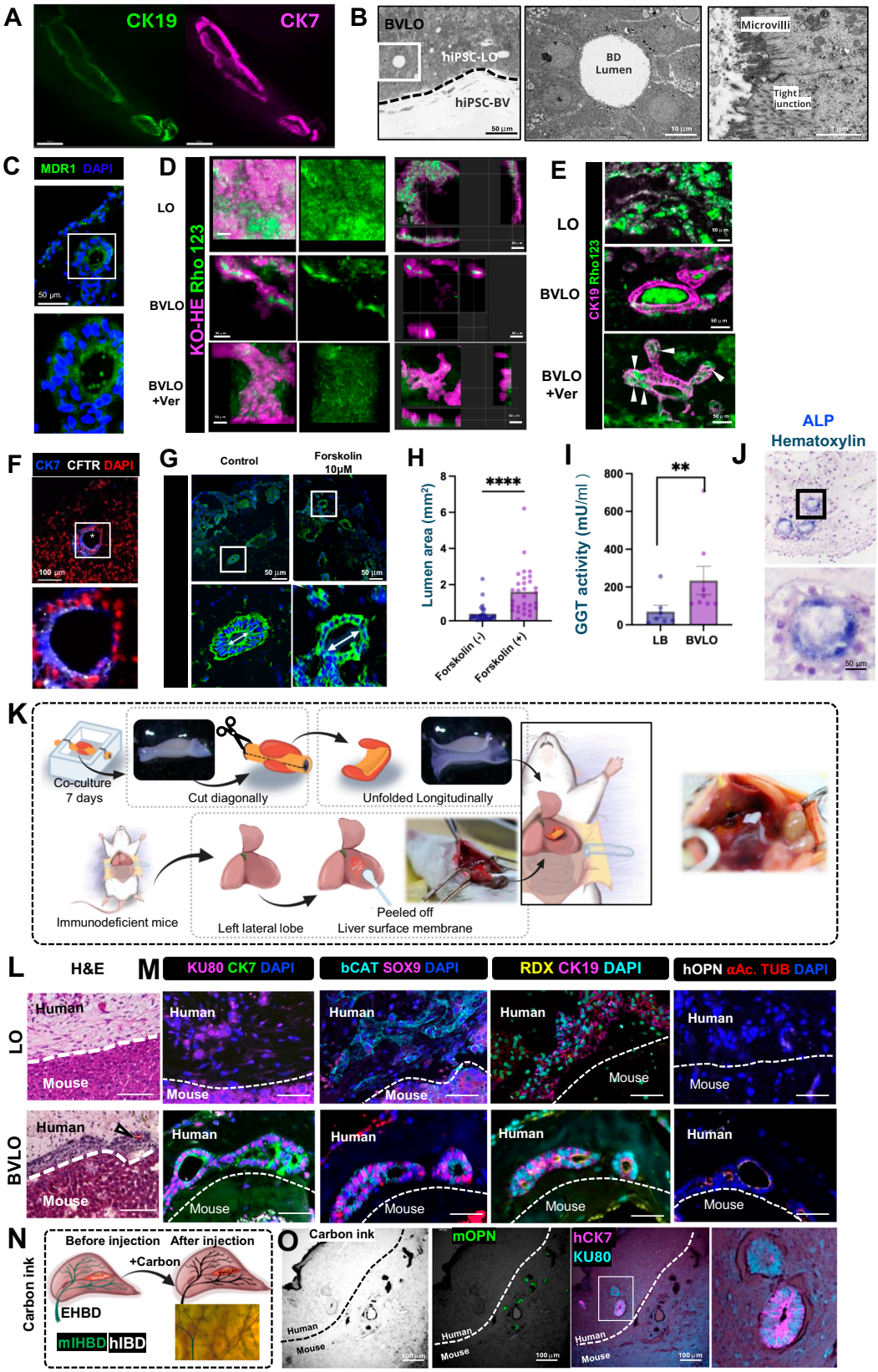

hiPSC-BDs. In short, the BVLO culture protocol enables the generation of functional hiPSC-BD lumen structures in vitro, which undergo further maturation post-transplantation. However, future study to optimize the protocol is necessary to achieve full BD maturation.

Our culture system presents a unique aspect to model human biliary diseases over traditional hiPSC-biliary organoid by enabling the modulation of BV-BD interaction through gene editing. As shown in Fig. 6, we can recapitulate bile duct paucity seen in Alagille syndrome by knocking out JAG1 in imSMC composing the BV. Notably, JAG1$^{-/-}$ hiPSCs-liver progenitors could still differentiate to cholangiocytes by interacting with JAG1 wild type hiPSC-imSMCs underscoring the versatility of the system. Given the possibility to modify each component

https://doi.org/10.1038/s41467-024-51487-3

Fig. 3 | In vitro and in vivo functionality characterization of BVLO. A 3D imaging demonstrates BVLO tubular structure. Scale bar: 100 µm. **B** TEM image of BVLO at varying magnifications. Scale bar: 50 µm, 10 µm, and 1 µm. Experiments were repeated independently two times with similar results. **C** Immunostaining of MDR1. Scale bar: 50 mm. Experiments were repeated independently two times with similar results. **D** Rho123 transport in hiPSC-BD without and with hiPSC-BV and the Verapamil. Scale bars: 50 µm. Experiments were repeated independently two times with similar results. **E** Immunostaining after Rho123 incubation showing luminal accumulation of Rho123 in the absence of verapamil. Scale bar: 50 µm. Experiments were repeated independently three times with similar results. **F** Immunostaining of CFTR. Scale bar: 100 µm. Experiments were repeated independently three times with similar results. **G** Immunofluorescence pre- and post-forskolin treatment. Scale bar: 50 µm. **H** Quantification of lumen area pre- and post-forskolin (Two-tailed Mann-Whitney test, Statistical significance ****P-value < 0.0001). Lumen area for BVLO with Forskolin ($n = 30$) and without ($n = 26$). Error bars represent SEM. **I** GGT activity assay of BVLO (Two-tailed Mann-Whitney test, Statistical significance **P-value of 0.0093). GGT activity of LO ($n = 7$) and BVLO ($n = 8$) was determined. Error bars represented SEM. **J** Alkaline phosphatase activity of hiPSC-BD after BCIP/NBT staining. Scale bar: 50 µm. Experiments were repeated independently more than three times with similar results, **K** Schematic overview of liver transplantation procedure. **L** Histological analysis of liver specimen rom NOG mice post-transplantation, H&E staining. Scale bar: 100 µm. Experiments were repeated independently more than three times with similar results. **M** Immunofluorescence analysis of LO, or BVLO post-transplantation. Cholangiocyte (CK19, SOX9, CK7, Ac. Tub, hOPN), epithelial junction and polarity markers (βCAT, RDX), human cell marker (Ku80) and a hepatocyte marker (HNF4A). Scale bar: 50 µm. Experiments were repeated independently more than three times with similar results. **N** Schematic illustration of carbon ink injection process from EHBD post-transplantation. **O** Bright field and fluorescence of carbon ink injection showing hCK7$^+$ human and mOPN$^+$ mouse BDs in the boundary transplanted area and the recipient area. Scale bar: 100 µm. Experiments were repeated independently more than three times with similar results.

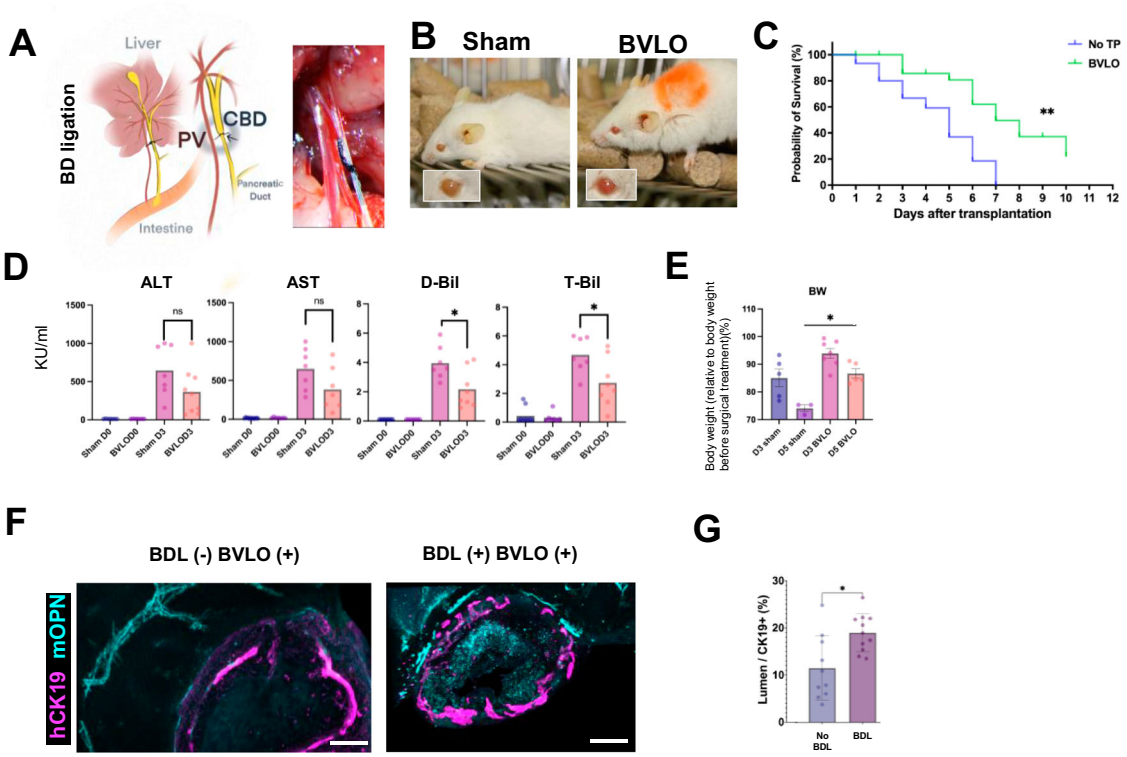

Fig. 4 | Temporarily improved survival of bile duct ligated mice model following BVLO liver surface transplantation. A Schematic illustration of common bile duct (CBD) ligation procedure to induce obstructive cholestasis. **B** Jaundice symptoms in NOG mice post-BDL, comparing non-transplanted or BVLO transplanted groups. **C** Survival rate of NOG mice post-BDL, comparing non-transplanted and BVLO-transplanted groups. Kaplan-Meier analysis with statistical significance assessed using the log-rank (Mantel-Cox), two-sided test, no adjustments were made for multiple comparisons. A p-value of 0.0034 was obtained. **D** Serum marker in BDL-ligated NOG mice: Non-Transplanted vs. BVLO transplanted. Evaluating alanine aminotransferase (ALT), aspartate aminotransferase (AST), direct-bilirubin (D-Bil), and total-bilirubin (T-Bil), (two-tailed Mann-Whitney test. ALT, ns; $p = 0.1067$, AST, ns; $p = 0.095$, D-Bil, Statistical significance *$p = 0.0311$, T-Bil, Statistical significance *$p = 0.0314$). Error bars represent SEM. **E** Percentage of body weight remaining in BDL-ligated NOG mice: Non-Transplanted vs. Transplanted (Two-tailed Mann Whitney test, statistical significance *$p = 0.0357$). Sham day 3 ($n = 5$), day 5 ($n = 3$) and BVLO transplanted day 3 (n = 7), day 5 ($n = 5$); Error bars are represented as SEM. **F** Wholemount immunofluorescence of thick liver slices post BDL and BVLO transplantation: BVLO non-transplanted vs BVLO-Transplanted group. Scale bar, 300 µm. **G** Quantification of graft' BD lumen area in BVLO-Transplanted NOG mice, BDL vs. Non-BDL (Two-tailed Mann Whitney test, Statistical significance *p-value of 0.0101). Three biological replicates were prepared and from each, three or four areas were selected in a thick section. Lumen areas were quantified using imageJ analysis software and error bars representing SEM.

of BVLO, this system offers a platform to scrutinize the etiology of other human BD aberrant formation.

Beyond disease modeling, hiPSC-BD holds promise for regenerative medicine application. Transplanting BVLO onto the liver surface of a cholestatic mouse has shown potential to temporarily alleviate cholestatic symptoms. The lumen continuity between hiPSC-BD and the host IHBD may enable BVLO to provide an additional reservoir to accommodate excess bile within the recipient's liver. Even though current benefit remains temporary and BVLO cannot completely resolve the obstruction in biliary diseases, it represents a step forward in managing cholestatic conditions.

From the perspective of liver tissue, aside of cholangiocytes and BDs, hepatocytes represent essential epithelial components of the liver. scRNAseq analysis of BVLO revealed that it contains ~13%

https://doi.org/10.1038/s41467-024-51487-3

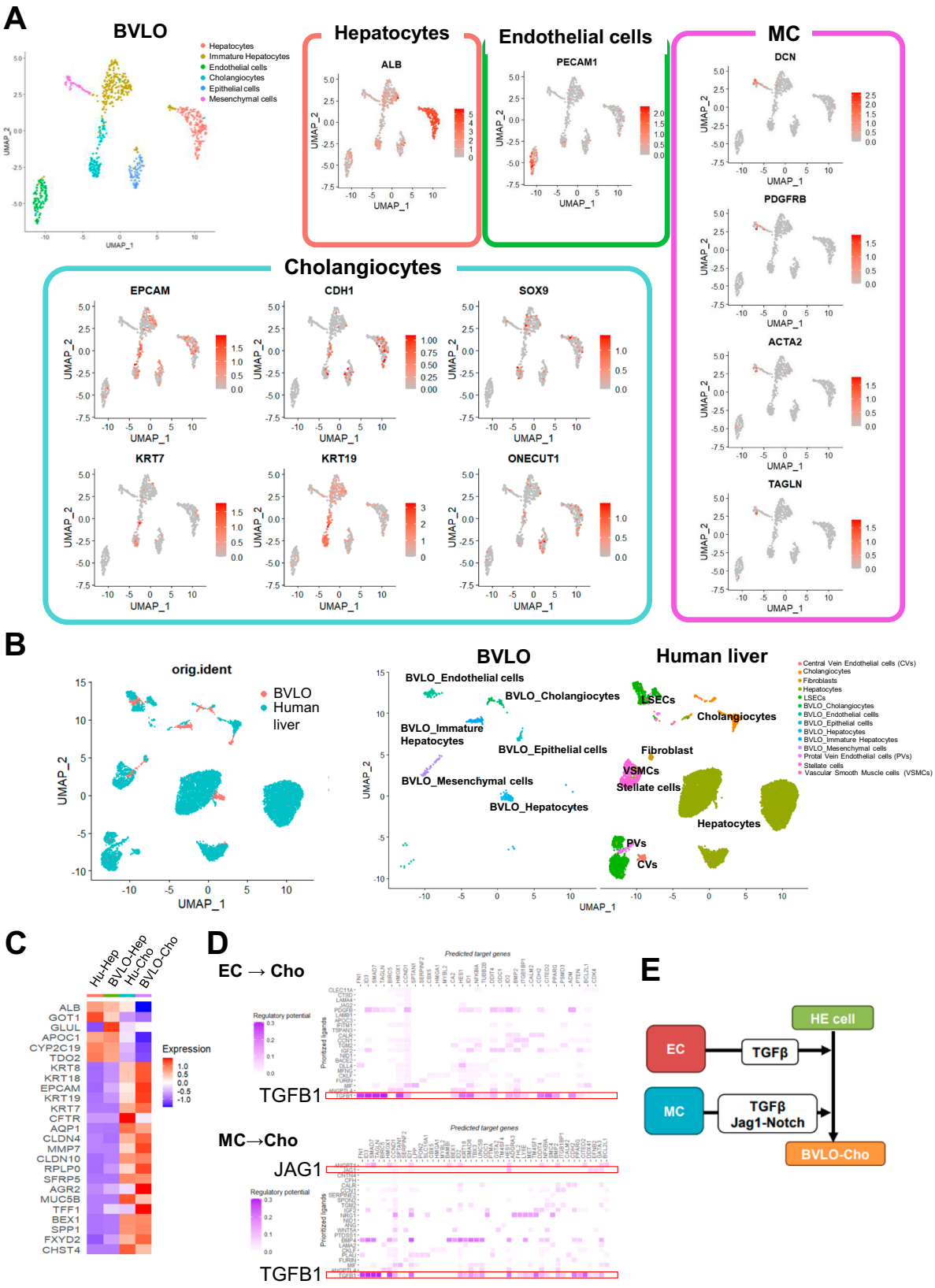

hepatocytes (Fig. 5). Those hepatocytes express hepatocyte marker genes, secrete albumin, and show xenobiotics metabolizing activity (Supplementary Fig. 11A–C). However, their structure remains immature, with a notable absence of bile canalicular network (Supplementary Fig. 11D). Thus, complementing current BVLO's BD graft-host connection with hepatobiliary network continuity will enable the development of liver tissue on a dish complete with an integrated end-to-end bile drainage system, in the future.

Our method of co-culturing epithelial organoids with an artificial BV offers the ability to derive complex liver structures in vitro, which are useful for modeling human biliary diseases. Given the pivotal role of BV in facilitating blood circulation to deliver nutrients and oxygen to

Fig. 5 | Single-cell transcriptome analysis demonstrates the PV-BD interactions in BVLO. A Single cell RNA-seq analysis of dissociated BVLO identified four distinct cell clusters; Hepatocyte cluster contains *ALB*$^+$ cells; Endothelial one contains *PECAM-1*+ cells; Cholangiocyte cluster contains *SOX9*$^+$, *EpCAM*$^+$, *KRT19*$^+$, *HES1*$^+$, *NOTCH1*$^+$, *NOTCH2*$^+$ cells; Mesenchymal cell cluster contains *ACTA2*$^+$, *TAGLN*$^+$, *PDGFRB*$^+$, *JAG1*$^+$ cells. In addition to these four clusters, part of BVLO component cells were annotated to immature hepatocytes or epithelial cells, which show hybrid phenotypes of cholangiocytes and hepatocytes. **B** Comparative clustering analysis of BVLO and human adult liver scRNA-seq data from "Human liver Cell Atlas" (GSE124395). This figure highlights the clustering proximity of cholangiocyte and hepatocyte within BVLO and human adult liver. **C** Heat map visualization of cholangiocyte and hepatocyte markers expressed in BVLO-derived cells compared to those in primary human liver cells highlights the similarities in the corresponding marker expression. **D** NicheNet analysis suggesting intercellular communication in BVLO. This ligand–target matrixes denote the regulatory potential between 25 ligands in Mesenchymal Cell (MC: upper) or Endothelial cell (EC: lower) and target genes in Org-Cho (the highly expressed genes in Org-Cho against planar cultured HE cells). As highlighted with red boxes, TGFβ1 in ECs and TGFβ1 as well as JAG1 in MCs potentially activate the corresponding downstream targets in cholangiocytes. **E** Schematic illustration of possible EC and MC contribution to the BVLO signaling pathways that are suggested to be associated with the differentiation of cholangiocyte clusters from HE cells in BVLO and formation of BD.

tissue/organ component cells, the integration of BV into organoids has been a recent target for many researchers. Finally, the current study shed light on another aspect of BV function: emulating BV-epithelial interaction could promote epithelial morphogenesis, facilitating the development of 3D physiologically functional tissue structures in human epithelial organoids.

Methods

Animals and cell culture

Pregnant female C57BL6 mice were purchased from Japan SLC INC (Tokyo Japan). Nonobese diabetic/Shi-scid, IL-2RγKO Jic (NOG) male mice (6–8 weeks old) were purchased from Clea, Japan, Inc. (Tokyo, Japan). All animal experiments were performed according to the ethical rules established by The Institute of Medical Science, The University of Tokyo animal experiment committee (PH5-13). All mice were housed under University of Tokyo animal center standard with a 12-h dark/light cycle, an ambient temperature of 22 ± 2 °C and a relative humidity of 50 ± 10%. The human iPSC (hiPSC) Ff-I01s04 and JAG1 KO lines[34] were kindly provided by Kyoto University and by Dr. Yohei Hayashi, Riken, Cell Bank, respectively. The use of hiPSCs was approved by the ethics committee of The University of Tokyo (2023-102-0305, 2023-101-0308). The fetal liver tissue (the estimated age of the fetus was gestation week 15 (GW15)) used in this work came from clinical abortion. The use of human fetal liver tissue by an opt-out consent was approved by the ethics committee of Asahikawa Medical University (22059) and that of the Institute of Medical Science, the University of Tokyo (2023-6-0518). Opt-out consent is a standard process in Japan to obtain human fetal tissue for research purposes.

Whole-mount fetal liver imaging

After the fetal liver was extracted from the main fetal body under a Leica M205 FA-Sony alpha 6000 microscope, the liver was fixed with 4% paraformaldehyde (PFA) overnight. Delipidation of the liver was done overnight to remove red blood cell residues and increase tissue transparency by using 10% CHAPS (Nacalai Tesque, Kyoto, Japan) and 25% N-methyldiethanolamine (NMDEA) solution (Sigma Aldrich, Missouri, USA) in a shaking water bath, at 37 °C. The CHAPS/NMDEA solution was replaced once the color had changed into green. Next, the fetal liver was washed with 0.1%Tween-PBS (PBST) three times, and proteins were blocked by incubating it with Protein Block Serum-free (DAKO, Jena, Germany) for 2 h at room temperature[35], on a shaker. First, the primary antibody was diluted and incubated for 5 days, at 4 °C, on a rotator. The following day, the liver was washed with PBST three times, every 60 min, on ice. The secondary antibody was diluted (1:500) and incubated for 2 days, at 4 °C, on a rotator. The fetal liver was then again washed with PBST post-incubation, three times, every 60 min, on ice. Tissue dehydration was done by serial dilution using methanol solution, and tissue clearing was performed using the BABB method as previously described[35] using a 1:1 mix of Benzyl Benzoate (Sigma Aldrich, Darmstadt, Germany) and Benzyl Alcohol (TCI, Tokyo, Japan). Images were taken with a Leica SP8 confocal microscope (Leica, Germany) and Olympus FVMPE-RS multiphoton microscope (Olympus, Tokyo, Japan). The staining and imaging experiments were independently replicated more than three times ($n = 3$) using liver lobes from different embryos to account for any variability.

Human induced pluripotent stem cell culture and liver bud generation

All hiPSC lines were maintained on dishes coated with Laminin 511E8 fragment (iMatrix-511TM, Nippi, Tokyo, Japan) in StemFit AK02N medium (Ajinomoto, Tokyo, Japan). Differentiation of hiPSC into HE, EC, and MC were done as described previously[3]. The generation of hiPSC-derived liver bud was carried out as described previously[4]. HE, EC, and MC harvested from planar culture were reseeded on a 24-well plate. Cell ratio of HE (5×10^5), EC (1×10^5), and MC (1×10^5) were seeded per well in an EZSPHERE® 24-well plate (Iwaki, Shizuoka, Japan). On the following day, two wells of EZSPHERE® 24-well plate liver organoid sphere were collected and reseeded on top of 0.4 μm porous membrane THINCERT® cell culture insert (Greiner, Frickenhausen, Germany) by using one well of silicone insert (ibidi, Lochhamer, Germany). AJI4/VEC-1 medium was used as a maintenance medium throughout the co-culture. AJI4 media comprises of DMEM (high glucose) (Fujifilm Wako, Osaka, Japan), 5% FBS (Biowest, Riverside, Missouri, USA), human OSM (20 ng/ml) (R&D System, Minneapolis, USA), Dexamethasone (Dex)(100 nM) (Sigma, St. Louis MO), Insulin (5 ng/ml) (Gibco), Hydrocortisone (0.5 μg/ml), holo-transferrin (10 μg/ml), Gentamycin (50 ng/ml) mixed with 1:1 ratio of VEC-1 medium (KOHJIN BIO, Saitama, Japan).

hiPSC-derived blood vessel generation

First, a 1 ml syringe (Terumo, Tokyo, Japan) was cut half in length, and then the smaller hole located in the head of the syringe was covered with Parafilm®. Next, a 1.5 ml tube containing 1×10^6 hiPSC-imSMC or hiPSC-mSMC cell pellet was prepared while 400 μl DMEM medium containing 5 μl 1 N NaOH was prepared in a separate tube. The recombinant protein, TGFß1 (10 ng/ml) (R&D Systems) and 1 μM Jagged-1 Fc (R&D Systems, Minneapolice, MN), were added to the tube containing DMEM medium (Fujifilm Wako, Osaka, Japan). 100 μl of rat collagen-1 (R&D System) was then added to DMEM-recombinant solution and mixed thoroughly. DMEM-collagen mixed solution was then added to the cell pellet. The final solution was transferred to a 1 ml syringe (Terumo, Tokyo, Japan), followingly, a 21 G needle (Terumo, Tokyo, Japan) was inserted to the middle of the solution to be incubated at 37 °C for 20 min—for gel solidification. Excess water was removed with a hydrophilic nylon membrane, 0.2 μm pore size (47 mm diameter) (Merck Millipore, Darmstadt, Germany) for another 20 min. Next, both sides of the SMC cell-containing vessel were attached to a soft catheter [Nipro safelet cath 26 G (Nipro, Osaka, Japan)] by creating ties using a 4 G surgical suture (Natsume, Tokyo, Japan). 1×10^6 hiPSC-EC pellet was resuspended in a 15 μl DMEM medium and drawn into a 20 μl microsyringe (Trajan, Victoria, Australia). The cell suspension was then inserted slowly into the lumen of the SMC cell-containing vessel tube through the aperture of the soft catheter, followed by incubation at 37 °C for 10 min. Then, the tube was reversed to ensure that the cell spread homogenously within the lumen, followed by a second incubation at 37 °C for 10 min. Finally, 100 μl of Miracell EC Culture medium (Takara, Shiga, Japan) was inserted into the lumen. The medium that

https://doi.org/10.1038/s41467-024-51487-3

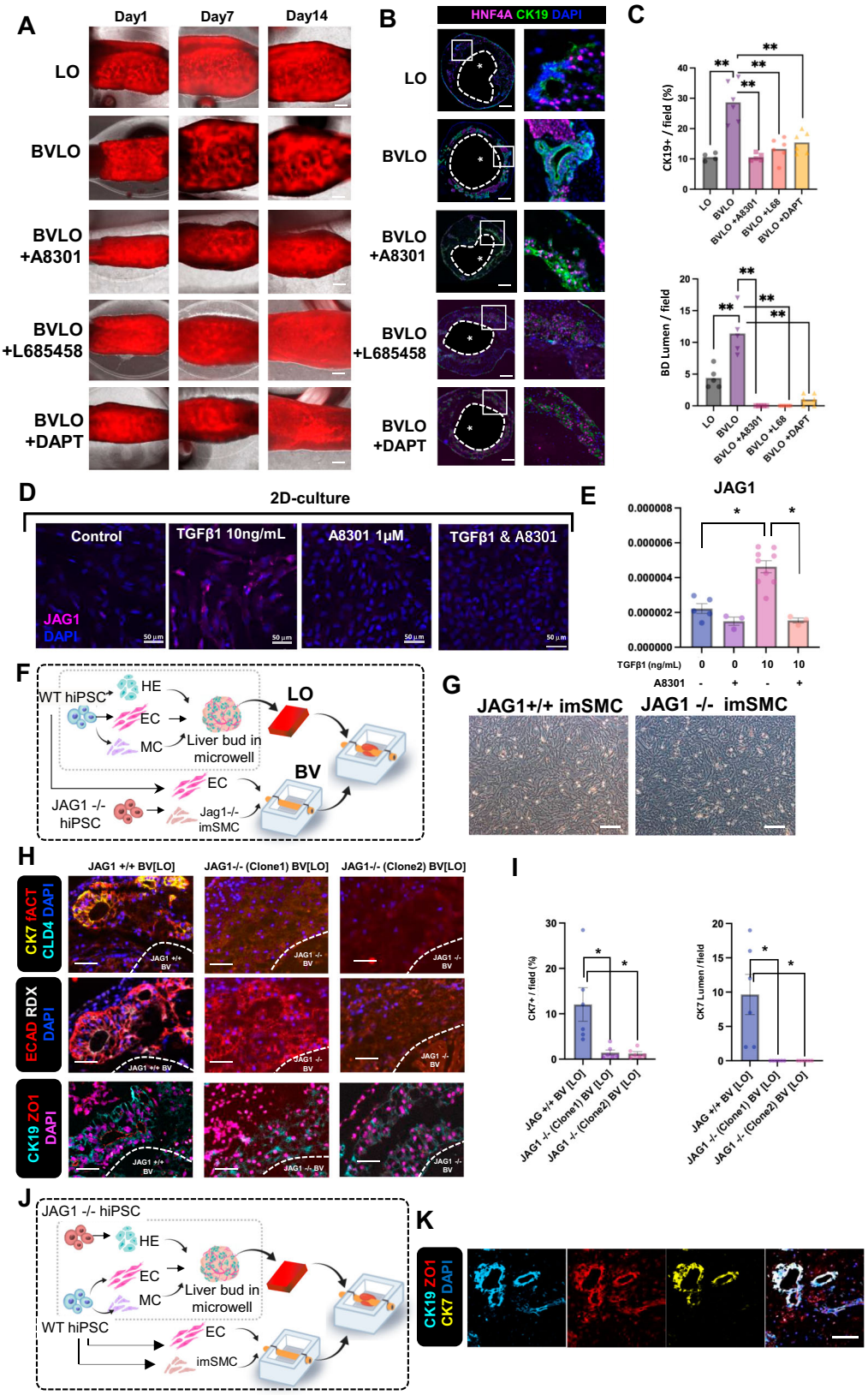

was used to culture EC on day 1 after the first passage was StemPro 34-SFM (Gibco), followed by Miracell medium as aforementioned.

The generation of BVLO

After aggregated liver organoid was overlaid surround hiPSC-derived BV, ECM with the composition of 9:1 Matrigel matrix Growth Factor Reduce (Corning, Bedford MA, USA) and Rat collagen-1 are used to coat the outer layer of the liver organoid. Laminin-511 5 μg/ml was added to the ECM mix for BVLO. Macroscopical observation was carried out using Nikon eclipse Ti -S, Nikon C-HGFI, and NIS-Elements BR 4.5 (Nikon, Tokyo, Japan). For setting the culture conditions, more than 3 organoids were generated for each combination of cells and

Fig. 6 | Dependency of bile duct formation within BVLO on JAG1/NOTCH which augmented by TGFB signal. A Representative phase-contrast and epi-fluorescence image of LO and BVLO containing KO-HE. KO-HE form a mesh-like network in BVLO, suppressed by A8301, L685458, or DAPT. Each experiment was repeated independently three times with similar result (Scale bar: 500 μm). **B** Imunofluorescence of LO, BVLO, or BVLO treated with A8301, L685458 or DAPT (scale bar: 200 μm). **C** Quantification of BD lumen number and CK19$^+$ area ratio in LO or BVLO treated with A8301, L685458 or DAPT. Culture was independently repeated for LO (n = 4), BVLO (*n* = 6), BVLO + A8301 (*n* = 5), BVLO + L685458 (*n* = 6), and BVLO + DAPT (*n* = 6). (Kruskal-Wallis test followed by Steel multiple comparison test, CK19$^+$ area with statistical significance **, **, **, ***P*-value of 0.0095; 0.0043; 0.0022; 0.0022), lumen number with statistical significance **,**,**,**,***P*-value of 0.0070; 0.0079; 0.0022; 0.0022. Error bars are SEM. **D** Immunofluorescence of JAG1 from planar-cultured imSMCs (Scale bar: 50 μm). **E** qPCR of JAG1 from planar-cultured SMCs. Sample number for control (*n* = 5), A8301 (*n* = 3), TGFβ1 (*n* = 9), and TGFβ + A8301 (*n* = 3). (Kruskal-Wallis with Steel multiple comparison test, TGFβ1:10 ng/ml vs TGFβ1:0 ng/ml, and TGFβ1:10 ng/ml vs TGFβ1:10 ng/ml+A8301:1 μM, Statistical significance: **P*-value of 0.0400; 0.0400). Error bars are SEM. **F** Schematic illustration of BVLO generation using JAG1 knock out-imSMC. **G** Bright field image of JAG1 knock-out iPSC-derived imSMCs (Scale bar 200 μm). **H** Immunofluorescence analysis of BVLO vs. two clones of JAG1 Knock-out imSMC BV[LO]. Cholangiocyte markers (CK19, CK7), epithelial junction and polarity markers (ZO1, ECAD, fACTIN, CLDN4, RDX). Culture was repeated three times, independently. For each set of culture, two BVLOs incorporating the BV with JAG1 + / +, JAG1−/− clone 1, and JAG1−/− clone 2 MCs were generated. Three to four fields from each organoid sample were analyzed. Scale bar 50 μm. **I** Quantification of CK7$^+$ area, and lumen number in BVLO vs. JAG1 knock-out imSMC BV[LO]. Three to four fields in two different sections of each organoid sample were analyzed for quantification. (Kruskal-Wallis with Steel multiple comparison test: **P*-value of 0.0022 and 0.0022). Error bars represent SEM. **J** Schematic illustration of BVLO generation using JAG1 Knock out-HE cells. **K** Immunofluorescence of BVLO containing JAG1 Knock-out HE cells (Scale bar: 100 μm). Cholangiocyte (CK19, CK7), epithelial markers (ZO1). Culture was repeated independently two times with similar result.

recombinant proteins. BVLO is an excellent system to emulate BD-BV interaction in vitro, but it needs a bit more training and experience than culturing hiPSC.

Flow cytometry sorting analysis

After 3 weeks of co-culture, the liver organoid was washed with PBS and sliced into smaller pieces using small surgical scissors. BVLO dissociation was done by incubation in digestion medium [0.5 mg/mL] collagenase (Sigma-Aldrich), 0.5 mg/mL pronase (Roche, Basel, Switzerland), and 0.25 mg/mL DNase1 (Sigma-Aldrich) in liver digestion medium[36] for 30 min at 37 °C, on shaker. Enzyme activity was stopped by the addition of 5% FBS in PBS. The dissociated cell solution was filtered with 40 μm mesh and inserted into a 15 ml tube. Next, centrifugation (400 × g) was carried out for 5 min to pellet the cells. 100 μl of 5% FBS in PBS was added to the tube. Alexa647-conjugated anti-EpCAM antibody (1 μl) (Biolegend) was added to the tube and incubated at 4 °C in the dark for 15 min. Cells were then washed with 5 ml 5% FBS in PBS. Cell sorting was performed with the FACSAria ™ III (BD biosciences, Franklin Lakes, New Jersey, USA). We repeated cell isolation from 2 or 3 BVLOs three times at each time point.

Liver organoid-dissociated cells were distinguished from debris on the flow cytometric profile based on the Forward Scatter (FSC) and Side Scatter (SSC). Cell aggregates were gated out based on their properties displayed on the SSC width (SSC-W) versus height (SSC-H) dot plot. Cells were then again gated in an FSC height (FSC-H) and FSC-area (FSC-A) dot plot to eliminate doublets. Living HE-derived cells within the organoid was recognized by Kusabira Orange positive population (PE). Hoechst staining was omitted for cell sorting due to increased toxicity and causing a minimum number of cell recovery. KO$^+$/EpCAM$^+$(APC$^+$) cells or particular cells of interest like GFP$^+$ BV cells were sorted on the basis of a IgG isotype control.

Gene expression qPCR analysis

RNA was extracted with PureLink™ RNA Mini Kit (Invitrogen, Waltham, Massachusetts, USA) from planar-cultured cells according to the manufacturer's protocol. PureLink™ RNA Micro Scale Kit (Invitrogen, Waltham, Massachusetts, USA) was used for RNA extraction from sorted cells. Total RNA was isolated and processed for reverse transcription (RT) with High-Capacity cDNA Reverse Transcription Kit (Applied Biosystems, Waltham, Massachusetts, USA) using Bio-Rad T100 Thermal Cycler (Hercules, California, USA). Real-time PCR reactions were carried out with the Universal Probe Library System (Roche Molecular Systems, Basel, Switzerland) using THUNDERBIRD® Probe qPCR Mix (TOYOBO, Saitama, Japan). 18S rRNA was used as reference genes. All probes and primers used for qPCR are presented in Supplementary Table 1. At least three independents total RNA was isolated for each group and qPCR was performed in duplicate for each RNA sample. The results are presented as the average of three technical replicates (*n* = 3) with standard deviation as error bar.

Bulk RNA sequencing (RNA-Seq)

RNA quality check was performed with 4150/4200 RNA screen tape (Agilent tech, Santa Clara, CA) kit. 5 μl of RNA sample buffer and 1 μl of RNA sample was added to each vial. Vortex homogenization was performed for 1 min, followed by incubation at 72 °C for 3 min, and then moved to the icebox for 2 min. RNA integrity was evaluated using Agilent 4200 tapestation (Agilent Technologies, Santa Clara, CA), and RNA samples with RNA integrity number > 8.8 were subjected for RNA-Seq analysis. RNA-seq libraries were prepared using 30 ng of total RNA with an Ion AmpliSeq Transcriptome Human Gene Expression kit (Thermo Fisher Scientific, Waltham, Massachusetts, United States) according to the manufacturer's instructions. The libraries were sequenced on the Ion Proton system using an Ion PI Hi-Q Sequencing 200 kit and Ion PI Chip v3 (Thermo Fisher Scientific), and the sequencing reads were aligned to hg19_AmpliSeq_Transcriptome_ERCC_v1 using Torrent Mapping Alignment Program. Subsequently, the data were analyzed using AmpliSeqRNA plug-in v5.2.0.3, a Torrent Suite Software v5.2.2 (Thermo Fisher Scientific), which provides QC metrics and normalized read counts per gene. Data were analyzed and visualized using the Subio platform (Subio, Kasugai, Japan). We performed GO and KEGG pathway analysis using the DAVID Bioinformatics Resource ver. 6.8. Our data is deposited in GEO (accession # GSE198888).

Single cell RNA-seq data processing and analysis

Processed scRNA-seq datasets of "primary fetal & adult human liver hepatic stellate cells" used in Fig. 1 were downloaded from the Single-cell atlas of human liver development reveals pathways directing hepatic cell fates" (https://collections.cellatlas.io/liver-development). scRNA-seq data of human liver used in Fig. 5 were downloaded from the "Liver Cell Atlas: Human CD45$^-$ cells" (https://www.livercellatlas.org/download.php)[37].

For scRNA-seq library preparation of BVLO, four BVLOs were dissociated to single cells by collagenase/pronase. The library was prepared using Chromium Single Cell 3' Reagent Kits (v3.1 Chemistry Dual Index) according to the manufacture's protocol (10×genomics, Pleasanton, CA). Sequence was performed by Macrogen Japan (Tokyo, Japan). The dataset is deposited in GEO (accession # GSE240019). For scRNA-seq analysis, the fastq file and gene count matrix are generated by cellranger-7.0.1. Downstream analysis is performed by Seurat v4[38]. The raw read counts generated by cellranger were filtered based on mitochondrial gene, feature number and RNA number (nCount_RNA ≤ 8000 & nCount_RNA ≥ 500 & nFeature_RNA ≤ 20000& nFeature_RNA ≥ 200 & percent.mt < 10 & 0.8 > log10(nFeature_RNA/nCount_RNA)), and then they were normalized by the normalization

method "NormalizeData". The top 2000 most variably expressed genes were used as the features of the dataset (FindVariableFeatures).

The corrected data were used for UMAP (RunUMAP function; reduction = "PCA", dims = 1:30). Resolutions of 0.7 (FindClusters function) were used for clustering. The clusters of interest were subset and compared for differential gene expression using the Wilcoxon rank-sum test (FindAllMarkers function) to identify marker genes or upregulated genes. Gene ontology analysis was performed using the clusterprofiler package. Genes upregulated in the selected clusters were obtained using the FindAllMarkers function, and the genes enriched in these clusters were subsequently analyzed for the enrichment of biological processes (BP) using the compareCluster function (function = enrichGO, ontology = BP, pvalueCutoff = 0.05).

Planar cultured HE and MC scRNA-seq datasets were from GSE270413. The integration of BVLO and other datasets (human liver atlas and planar cultured cells) was achieved by the "anchor-based" integration workflow. Differentially expressed genes in BVLO cholangiocytes against planar-HE were used as the "target genes" for NicheNet cell-cell interaction inference analysis[31].

Whole-mount organoid imaging

Liver organoids were washed with PBS once and then fixed with 2% PFA. Organoids were blocked with Dako-protein blocking solution (Dako Agilent, Santa Clara, CA) for 2 h at room temperature on top of the shaker (Taitec, Saitama, Japan). Samples were incubated with primary antibody listed in Supplementary Table 2 at 4 °C overnight on a rotator. The following day samples were washed three times with PBST, and secondary antibody solution (Invitrogen, Thermo Fisher Scientific) was incubated at 4 °C overnight on a rotator. Again, the samples were washed three times with PBST the following day. The nuclei were stained with 4′, 6-diamidino-2-phenylindole (DAPI) solution (Nacalai Tesque, Kyoto, Japan). Afterwards tissue clearing methods were performed using CUBIC-R (TCI, Tokyo, Japan). The whole mount staining with each set of primary antibodies was repeated more than twice and the representative images were shown in Fig. 3A and Supplementary Video 1.

Immunofluorescence analysis

The organoids were fixed with 2% PFA and washed one time with PBS. Frozen blocks were made using OCT compound (Sakura Finetek, Tokyo, Japan) and frozen using liquid nitrogen on cryomold number 2 (Sakura Finetek, Tokyo, Japan). A thin frozen section (5–9 μm) was made using CryoStar NX70 Cryostat (Thermo Scientific). Then, the slices were dried, washed three times using PBS, blocked with protein serum-free block, and incubated with primary antibody at 4 °C overnight. The next day, the samples were washed three times with PBS, and a secondary antibody was added and kept at room temperature for 1 h. The nuclei were stained with DAPI solution (Nacalai). Lastly, the organoid was mounted with Apathy's Mounting Media, Soluble (Wako, Osaka, Japan) and covered with cover glass (Matsunami, Bellingham, WA). Slides were prepared from more than three independent biological replicates. Images were taken with Leica DMi8 microscope, with the addition of Leica DFC 7000 T and Leica DFC 9000 GTC camera.

Rhodamine assay

The liver organoid culture medium was removed and washed once with PBS. The liver organoid was then cultured with a fresh culture medium containing 100 μM Rhodamine123 (Fujifilm Wako, Osaka, Japan) for 60 min or together with 10 μM Verapamil Hydrochloride (Fujifilm Wako, Osaka, Japan). The liver organoid was then washed with a fresh culture medium overnight, followed by washing three times with a fresh culture medium the following day. Confocal microscopy imaging using Leica Sp8 (Leica Microsystems) was performed live after the liver organoid was cut longitudinally on top of the glass. For each experimental condition, the assay was repeated three times, independently and the representative images were shown in Fig. 3.

Forskolin -induced swelling assay

The liver organoid culture medium was removed and washed once with PBS. The liver organoid was divided into two parts, one part is fixed with 2% PFA, and the second part is treated with forskolin. Fresh culture medium containing10 μM forskolin was added to the mold chamber and incubated at 37 °C for 90 min. Macroscopical imaging was performed after 90 min, and the liver organoid was fixed with 2% PFA. Immunofluorescence analysis of both samples was then performed accordingly. The assay was repeated twice, and the duct structures were identified on frozen sections. More than 25 luminal structures were analyzed for their diameters.

Alkaline phosphatase activity via BCIP/NBT staining

Frozen sections were dried out and were circled with a hydrophobic marker, ImmEdge Pen (Vector Laboratories, Burlingame, California, USA). Sections were washed three times with PBS containing 0.1% PBST. For every 5 ml of alkaline phosphatase buffer (100 mM Tris-HCl [pH 9.0], 150 mM NaCl, and 1 mM $MgCl_2$), 33 μl NBT color development substrate (Promega, USA) and 16.5 μl BCIP were added. After mixing the solution well, it was added to the slides and incubated for 5 min, followed by dehydration with series of ethanol and xylene. Finally, sections were mounted with a quick–mount solution (Daido Sangyo, Kawasaki, Japan). The ALP enzymatic activity staining was repeated using several sections prepared from more than three independent BVLOs.

Inhibition of Notch and TGFB signal in BVLO

BVLOs were generated in the presence of A8301, L685458, and DAPT. Medium containing them was replated every 2 days. Cultures were repeated three times, independently. One JAG1 + /+ and two $JAG1^{-/-}$ -hiPSC clones (We acknowledge Dr. Yohei Hayashi from Riken Bioresource research center for providing these valuable samples) were induced to differentiate to imSMCs and used for preparing the BVs, which were cocultured with the sheet shape liver organoid to generate BVLOs. For each clone, cell differentiation and co-cultures were repeated three times, independently and more than three BVLOs were generated for each clone.

Mouse transplantation procedure

Transplantation was done 1 week after in-vitro co-culture. A combination anesthetic solution (M/M/B: 0.3/4/5) containing 0.3 mg/kg of medetomidine, 4.0 mg/kg of midazolam, and 5.0 mg/kg of butorphanol[39] was used to anesthetize the mice. Next, the mice peritoneum was opened, and the mesothelium membrane from the left liver lobe was peeled off using a sterilized cotton bud. Longitudinally unfolded liver organoid was transplanted to the peeled-off portion with liver organoid side facing bottom side and blood vessel side facing the upper side. After transplantation, liver organoid was covered by returning the middle lobe on top of it, and the peritoneum was closed using a 4 G suture. The transplantation experiments were independently replicated more than three times ($n > 5$) to account for any variability.

Mice cholestatic model was performed by surgical ligation of the common bile duct. First, mouse was anesthetized with 4% isoflurane at a flow rate of 1.3-2 L/ min for anesthesia induction. Mouse abdominal fur was shaved with an electric shaver and plated on a 37 °C heated hot plate. While anesthesia is maintained, abdomen skin is sterilized and cut opened by midline laparotomy of ~3 cm. The peritoneum was then cut to open peritoneal cavity. Expose the bile duct by caudal movement of the gut. Locate the pancreatic duct and place 6–0 suture around the common bile duct over the pancreatic duct. Ligate common bile duct with two surgical knots without dissecting the bile duct in between. Moisturize the peritoneal cavity with 0.9% NaCl and lift the liver over the Gut. Following this, the liver organoid was transplanted in the surface of the liver as aforementioned. A total of 16 mice were used for the cholestatic mice model transplantation experimented,

consisting of seven and nine mice were used for the No TP (BDL) and the BVLO group (BDL and BVLO transplantation).

Histological analysis

Tissue-Tek VIP 3 JR and Tissue-Tek®TEC™ (Sakura Finetek, Torrance, CA) were used to embed the transplanted liver tissue in a paraffin block after being fixed with 10% formaldehyde. Paraffin block was sliced at 7–9 μm (Thermo Scientific HM 340E, Waltham, Massachusetts, USA) and was deparaffinized with xylene three times, continued by washing with series of ethanol. Next, it was stained with hematoxylin (Muto Pure Chemicals, Tokyo, Japan) for 3 min and washed with tap water for 10 min. Counterstaining was done with eosin (Muto Pure Chemicals, Tokyo, Japan) and then dehydrated with series of ethanol and xylene. Finally, it was mounted with a quick–mount solution. Each experimental group was sectioned and stained in triplicate, resulting in a total of nine histological sections and representative picture is as shown in figure.

Statistical analysis

ImageJ 1.52a software (National Institutes of Health, Bethesda, MD) was used for all imaging analyses. GraphPad Prism 8 software (GraphPad Software, San Diego, CA) was utilized for statistical analysis, and EZR (Easy R)[40] for 2D-planar culture MC qPCR analysis. The results were expressed as means ± standard error (SEM) of independent experiments. All experiments were performed at least three times independently, and statistical significance was assessed by the nonparametric Mann–Whitney U test for gene expression analyses and forskolin quantification. P values of ≤ 0.05 were statistically significant.

Reporting summary

Further information on research design is available in the Nature Portfolio Reporting Summary linked to this article.

Data availability

The bulk and scRNA sequencing data generated in this study have been deposited in the GEO database under accession code GSE240534 (subseries: GSE198888, GSE240019, and GSE270413). The source data generated in this study both for main figures and extended figures are provided in the source data file with this paper. Source data are provided with this paper.

References

1. Esteller, A. Physiology of bile secretion. *World J. Gastroenterol.* **14**, 5641–5649 (2008).
2. Li, M. K. & Crawford, J. M. The pathology of cholestasis. *Semin Liver Dis.* **24**, 21–42 (2004).
3. Takebe, T. et al. Massive and reproducible production of liver buds entirely from human pluripotent stem cells. *Cell Rep.* **21**, 2661–2670 (2017).
4. Takebe, T. et al. Vascularized and functional human liver from an iPSC-derived organ bud transplant. *Nature* **499**, 481–484 (2013).
5. Takahashi, Y., Sekine, K., Kin, T., Takebe, T. & Taniguchi, H. Self-condensation culture enables vascularization of tissue fragments for efficient therapeutic transplantation. *Cell Rep.* https://doi.org/10.1016/j.celrep.2018.03.123 (2018).
6. Ogawa, M. et al. Directed differentiation of cholangiocytes from human pluripotent stem cells. *Nat. Biotechnol.* https://doi.org/10.1038/nbt.3294 (2015).
7. Sampaziotis, F. et al. Cholangiocytes derived from human induced pluripotent stem cells for disease modeling and drug validation. *Nat. Biotechnol.* https://doi.org/10.1038/nbt.3275 (2015).
8. Hayashi, H. et al. Modeling human bile acid transport and synthesis in stem cell-derived hepatocytes with a patient-specific mutation. *Stem Cell Rep.* **16**, 309–323 (2021).
9. Dianat, N. et al. Generation of functional cholangiocyte-like cells from human pluripotent stem cells and HepaRG cells. *Hepatology* **60**, 700–714 (2014).
10. Tian, L., Deshmukh, A., Ye, Z. & Jang, Y. Y. Efficient and controlled generation of 2D and 3D Bile duct tissue from human pluripotent stem cell-derived spheroids. *Stem Cell Rev. Rep.* **12**, 500–508 (2016).
11. Hofmann, J. J. et al. Jagged1 in the portal vein mesenchyme regulates intrahepatic bile duct development: insights into Alagille syndrome. *Development* **137**, 4061–4072 (2010).
12. Strazzabosco, M. & Fabris, L. Development of the bile ducts: essentials for the clinical hepatologist. *J. Hepatol.* **56**, 1159–1170 (2012).
13. Ramesh Babu, C. S. & Sharma, M. Biliary tract anatomy and its relationship with venous drainage. *J. Clin. Exp. Hepatol.* **4**, S18–S26 (2014).
14. Georgijevic, S. et al. Spatiotemporal expression of smooth muscle markers in developing zebrafish gut. *Dev. Dyn.* **236**, 1623–1632 (2007).
15. Tanimizu, N. et al. Intrahepatic bile ducts are developed through formation of homogeneous continuous luminal network and its dynamic rearrangement in mice. *Hepatology* https://doi.org/10.1002/hep.28521 (2016).
16. Antoniou, A. et al. Intrahepatic bile ducts develop according to a new mode of tubulogenesis regulated by the transcription factor SOX9. *Gastroenterology* **136**, 2325–2333 (2009).
17. Popescu, D. M. et al. Decoding human fetal liver haematopoiesis. *Nature* **574**, 365–371 (2019).
18. Patsch, C. et al. Generation of vascular endothelial and smooth muscle cells from human pluripotent stem cells. *Nat. Cell Biol.* **17**, 994–1003 (2015).
19. Atchison, L., Zhang, H., Cao, K. & Truskey, G. A. A tissue engineered blood vessel model of Hutchinson-Gilford progeria syndrome using human iPSC-derived smooth muscle cells. *Sci. Rep.* **7**, 1–12 (2017).
20. Camp, J. G. et al. Multilineage communication regulates human liver bud development from pluripotency. *Nature* **546**, 533–538 (2017).
21. Ayabe, H. et al. Optimal hypoxia regulates human iPSC-derived liver bud differentiation through intercellular TGFB signaling. *Stem Cell Rep.* **11**, 306–316 (2018).
22. Clotman, F. et al. Control of liver cell fate decision by a gradient of TGFβ signaling modulated by Onecut transcription factors. *Genes Dev.* **19**, 1849–1854 (2005).
23. Tanimizu, N., Kikkawa, Y., Mitaka, T. & Miyajima, A. α1- and α5-containing laminins regulate the development of bile ducts via β1 integrin signals. *J. Biol. Chem.* https://doi.org/10.1074/jbc.M112.350488 (2012).
24. Takayama, K. et al. Laminin 411 and 511 promote the cholangiocyte differentiation of human induced pluripotent stem cells. *Biochem. Biophys. Res. Commun.* https://doi.org/10.1016/j.bbrc.2016.04.075 (2016).
25. Tabibian, J. H., Masyuk, A. I., Masyuk, T. V., O'Hara, S. P. & LaRusso, N. F. Physiology of cholangiocytes. *Compr. Physiol.* **3**, 541–565 (2013).
26. Beekman, J. M. Individualized medicine using intestinal responses to CFTR potentiators and correctors. *Pediatr. Pulmonol.* **51**, S23–S34 (2016).
27. Dekkers, J. F. et al. A functional CFTR assay using primary cystic fibrosis intestinal organoids. *Nat. Med.* **19**, 939–945 (2013).
28. Rao, R. & Samak, G. Bile duct epithelial tight junctions and barrier function. *Tissue Barriers* **1**, e25718 (2013).
29. Fornaciari, I. et al. Gamma-glutamyltransferase fractions in human plasma and bile: characteristic and biogenesis. *PLoS One* **9**, 2–8 (2014).

30. Kaneko, K., Kamimoto, K., Miyajima, A. & Itoh, T. Adaptive remodeling of the biliary architecture underlies liver homeostasis. *Hepatology* **61**, 2056–2066 (2015).
31. Browaeys, R., Saelens, W. & Saeys, Y. NicheNet: modeling intercellular communication by linking ligands to target genes. *Nat. Methods* **17**, 159–162 (2020).
32. Pritchett, J. et al. Osteopontin is a novel downstream target of SOX9 with diagnostic implications for progression of liver fibrosis in humans. *Hepatology* **56**, 1108–1116 (2012).
33. Whitington, P. F. et al. Expression of osteopontin correlates with portal biliary proliferation and fibrosis in biliary atresia. *Pediatr. Res* **57**, 837–844 (2005).
34. Song, D. et al. Generation of human induced pluripotent stem cell lines carrying homozygous JAG1 deletions. *Stem Cell Res* **57**, 102588 (2021).
35. Yokomizo, T. et al. Whole-mount three-dimensional imaging of internally localized immunostained cells within mouse embryos. *Nat. Protoc.* **7**, 421–423 (2012).
36. Matsui, S. et al. Characterization of peribiliary gland–constituting cells based on differential expression of trophoblast cell surface protein 2 in biliary tract. *Am. J. Pathol.* **188**, 2059–2073 (2018).
37. Aizarani, N. et al. A human liver cell atlas reveals heterogeneity and epithelial progenitors. *Nature* **572**, 199–204 (2019).
38. Hao, Y. et al. Integrated analysis of multimodal single-cell data. *Cell* **184**, 3573–3587.e29 (2021).
39. Kawai, S., Takagi, Y., Kaneko, S. & Kurosawa, T. Effect of three types of mixed anesthetic agents alternate to ketamine in mice. *Exp. Anim.* **60**, 481–487 (2011).
40. Kanda, Y. Investigation of the freely available easy-to-use software 'EZR' for medical statistics. *Bone Marrow Transpl.* **48**, 452–458 (2013).

Acknowledgements

We would like to thank all members of the division of regenerative medicine for providing technical support. We thank the FACS core laboratory IMSUT for kindly providing technical support for cell sorting. We also thank EVIDENT CORPORATION for technical assistance in acquiring images with multiphoton microscope at TOBIC (The University of Tokyo IQB Olympus Bioimaging Center). This work was supported by the Japan Agency for Medical Research and Development (AMED) (JP13bm0304002, JP21fk0210073, and JP23bm1223007 to H.T., JP20gm6210029 and JP23bm1423025 to N.T.), and Ministry of Education, Culture, Sports, Science, and Technology (MEXT) (21H04830 to H.T., 20K05843, 23K18572, and 23H02967 to N.T., 19K18034 to Y.K.). This work is also supported by a Research Grant from the Orange Fund for the Commemoration of Hokkaido Hepatitis B Lawsuits to N.T. We also thank Enago (www.enago.jp) for the English language review.

Author contributions

E.C., Y.K., N.T. conceived and designed the study; E.C., N.T. wrote the manuscript with the input from Y.K; E.C., Y.K., A.O., K.A., S.M., E.K., T.O., S.Y., T.K., Y.N., K.Y., Y.F., N.T. performed all experiments; N.T., T.T., H.T. provided intellectual support; Y.K., N.T., H.T. acquired funding; All authors have read and agreed to the published version of the manuscript.

Competing interests

The authors declare no competing interests.

Additional information

Supplementary information The online version contains supplementary material available at https://doi.org/10.1038/s41467-024-51487-3.

Correspondence and requests for materials should be addressed to Naoki Tanimizu or Hideki Taniguchi.

Peer review information *Nature Communications* thanks the anonymous reviewers for their contribution to the peer review of this work. A peer review file is available.